Helios Spacecraft Low-Gain Antenna Model

N. C. Ham
R. F. Systems Development Section

An extension of the Helios spacecraft low-gain antenna analysis has been performed with emphasis on the region of RF signal interferometry produced by the combined signals radiated from the horn and dipole antennas of like polarization. A mathematical model of the low-gain antenna model is developed and resultant computer plots compared against the amplitude and phase characteristics measured from a spacecraft antenna mockup. The model proved to correlate well with measured patterns and serves to consider major effects that may impact the telecommunications link.

I. Introduction

The preliminary investigation of the Helios low-gain antenna (LGA) effect on a telemetry link was covered by Ref. 1 with particular emphasis on the effects due to amplitude modulation and frequency modulation upon the radiated carrier signal as the Helios LGA was rotated about its spin axis.

Reference 2 was an extension of the study following receipt of preliminary spacecraft LGA patterns measured from a Helios spacecraft mockup and for the condition of right circular polarization (RCP) at the deep space stations and was analyzed that the maximum frequency deviation would be 28 Hz with a frequency rate of change of 89 Hz/s.

Figure 1 illustrates the Helios spacecraft LGA coordinate configuration showing the combined RCP horn and linear dipole antennas which comprise the LGA that produces a typical polar gain pattern.

This report is a further extension of the LGA analysis with particular emphasis on the region of signal interferometry produced by the combined horn and dipole antenna of similar polarization and develops a mathematical model of the LGA and then compares the results against the extensive antenna pattern measurements contained in Ref. 3.

II. Mathematical Model of LGA

The dimensional configuration of the Helios LGA for mathematical modeling purposes is depicted in Fig. 2 for the downlink frequency of 2295 MHz, where the aspect angle ψ is set to 45° for mathematical expediency since the slope of the signal rays, $\cos \omega_c t$ and $\cos (\omega_c t + \beta)$, are -1 and the equal wave front line is 1.

Figure 2a is the three-axis orientation illustrating the RCP horn antenna rotating around the Z-axis and the dipole antenna, with its linear polarization, coaxial to the Z-axis. The RCP horn signal linear polarization component is obtained by projection to the X–Z plane to match the polarization of the dipole antenna within this same plane.

Next the two matched polarized signals will be considered as having a common wave front for a specific aspect angle ψ and then vectorily summed as a function of the rotation angle ϕ.

As a first approximation for this model, the ratio of the radiated signal form will be used to circumvent the tedious and detailed equations to account for changing ellipticity, fringe effects, etc.

Figure 2b is the diagram used to formulate the equation for summing the linear components within the X–Z plane. Simultaneous equations are derived as follows:

$$z = x + 6.5\lambda \cos \phi$$

$$z = -x + 30\lambda$$

and are solved to determine the coordinates (x_1, z_1) with resulting values of

$$x_1 = 15\lambda - 3.25\lambda \cos \phi$$

$$z_1 = 15\lambda + 3.25\lambda \cos \phi$$

The distance L represents the phase difference between the two signal sources as a function of the rotation angle ϕ. The value L from the above equations is

$$L = [(x_2 - x_1)^2 + (z_2 - z_1)^2]^{1/2}$$

$$L = [225\lambda^2 - 97.2\lambda^2 \cos \phi + 10.5\lambda^2 \cos^2 \phi + 225\lambda^2 - 97.2\lambda^2 \cos \phi + 10.5\lambda^2 \cos^2 \phi]^{1/2}$$

$$L = 4.6\lambda\,[21.4 - 9.25 \cos \phi + \cos^2 \phi]^{1/2}, \text{ wavelengths} \quad (1)$$

To express in phase angle at the carrier frequency, where $\lambda = 360°$, the equation becomes

$$L = 1660°\,(21.4 - 9.25 \cos \phi + \cos^2 \phi)^{1/2}, \text{ degrees} \quad (2)$$

L_0 is the reference distance at $\phi = 0°$ and equals 5800°, and as ϕ increases in magnitude, when the spacecraft is rotated as shown, the signal radiated from the horn antenna begins to lead the dipole signal by the phase angle β; or $\beta' = L - L_0$. However, as the horn antenna is rotated one revolution, the radiated E vector also undergoes one revolution, thus advancing an additional λ (or 360°) modifying the phase difference to become $\beta = \beta' + \phi$; hence,

$$\beta = 1660°\,(21.4 - 9.25 \cos \phi + \cos^2 \phi)^{1/2} + \phi - 5800°, \text{ degrees} \quad (3)$$

The general expression for the ground received signal, in terms of amplitude and phase, is the sum of the signal from the two LGA sources and is derived from the following diagram:

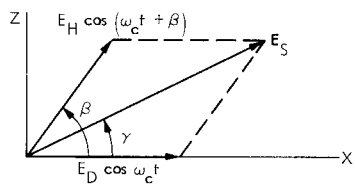

$$\mathbf{E}_S = \mathbf{E}_H + \mathbf{E}_D$$

where E_H is the horn signal and E_D the dipole signal,

$$\mathbf{E}_S = [(E_H \cos \beta + E_D)^2 + (E_H \sin \beta)^2]^{1/2}$$

and, finally, by normalizing the signal relative to the dipole antenna gain, as

$$E_S \angle \gamma = E_D \left[1 + \left(\frac{E_H}{E_D} \right)^2 + 2 \left(\frac{E_H}{E_D} \right) \cos \beta \right]^{1/2} \angle \arctan \left(\frac{\frac{E_H}{E_D} \sin \beta}{1 + \frac{E_H}{E_D} \cos \beta} \right) \tag{4}$$

Using the value of β from Eq. (3) and trigonometric identities, the general equation becomes

$$E_S \angle \gamma = E_D \left\{ 1 + \left(\frac{E_H}{E_D} \right)^2 + 2 \left(\frac{E_H}{E_D} \right) \cos \left[1660^\circ (21.4 - 9.25 \cos \phi + \cos^2 \phi)^{1/2} + \phi - 5800^\circ \right] \right\}^{1/2}$$
$$\angle \arctan \left(\frac{\frac{E_H}{E_D} \sin \left[1660^\circ (21.4 - 9.25 \cos \phi + \cos^2 \phi)^{1/2} + \phi - 5800^\circ \right]}{1 + \frac{E_H}{E_D} \cos \left[1660^\circ (21.4 - 9.25 \cos \phi + \cos^2 \phi)^{1/2} + \phi 5800^\circ \right]} \right) \tag{5}$$

for the specific aspect angle $\psi = 45^\circ$.

III. Signal Amplitude

The amplitude variation of the received signal as a function of the rotation angle ϕ, for the specific aspect angle $\psi = 45^\circ$, is the amplitude portion of the general equation (5):

$$E_S = E_D \left\{ 1 + \left(\frac{E_H}{E_D} \right)^2 + 2 \left(\frac{E_H}{E_D} \right) \cos \left[1660^\circ (21.4 - 9.25 \cos \phi + \cos^2 \phi)^{1/2} + \phi - 5800^\circ \right] \right\}^{1/2} \tag{6}$$

Figure 3a is the computer plot of the signal amplitude for values of $E_H = E_D = 1$, where the amplitude is in volts; Fig. 3b shows the results when the amplitude scale is the logarithm or in dB.

Figures 4a, 4b, and 4c are the dB plots for the values of $E_H = 0.8$, $E_D = 1.1$; $E_H = 0.9$, $E_D = 1.05$, and $E_H = 1.1$, $E_D = 0.9$, and are estimated average antenna gain values at $\psi = 47^\circ$, 46°, and 44°, respectively.

IV. Signal Phase

The phase variation of the received signal can be obtained in a similar manner from the general equation (5):

$$\gamma = \arctan \left(\frac{\frac{E_H}{E_D} \sin \left[1660^\circ (21.4 - 9.25 \cos \phi + \cos^2 \phi)^{1/2} + \phi - 5800^\circ \right]}{1 + \frac{E_H}{E_D} \cos \left[1660^\circ (21.4 - 9.25 \cos \phi + \cos^2 \phi)^{1/2} + \phi - 5800^\circ \right]} \right) \tag{7}$$

The ideal interferometry condition, when $E_H = E_D = 1$ (i.e., equal gain pattern from the dipole and horn antenna) for all rotation angle ϕ, is shown in Fig. 5 at the aspect angle of 45°, while Fig. 6 is for the value of $E_H = 0.7$ and $E_D = 1$. Figure 7 is for $E_H = 1.08$ and $E_D = 1$.

As can be seen in Fig. 5, the phase derivation about the received signal is $\pm 90^\circ$ for the condition $E_H/E_D = 1$ since Eq. (4) becomes

$$\gamma = \arctan \frac{\sin \beta}{1 + \cos \beta} = \arctan \cdot \tan \frac{1}{2} \beta = \frac{1}{2} \beta \tag{8}$$

Thus, when $\phi = 180^\circ$, $\beta = 90^\circ$ maximum, and when $\phi \simeq 181^\circ$, $\beta = -90^\circ$ maximum.

For the condition when $E_H/E_D = 0.7$, the phase deviation is seen to be approximately $\pm 46^\circ$; while for $E_H/E_D = 1.08$, the phase deviation is approximately $\pm 150^\circ$.

V. Actual Case Versus Ideal Case

The ideal case of equal amplitude from the LGAs for every value of ϕ at any specific aspect angle ψ does not

exist for the Helios configuration due to the offset horn antenna and slight physical misalignment of the dipole antenna from the spin axis and is further compounded when viewed at various aspect angles.

Figure 8 illustrates the polar plot of the LGA in the X–Z plane for the rotation angle $\phi = 0°$, which shows that for $\psi = 0°$ to 44° the horn antenna is dominant, while for $\psi = 53°$ to 180° the dipole becomes dominant, and $\psi = 44°$ to 53° is the combined horn–dipole region.

Figure 9 illustrates the orthogonal X–Y plane conic section for $\phi = 0°$ to 360° at various aspect angles.

Figure 10 is the test measurement configuration used to obtain the amplitude and phase characteristics from a Helios spacecraft mockup, and Fig. 11 is a reproduction of a typical measurement. This illustrates that $30° > \phi > 310°$ is the dipole region, $30° < \phi < 200°$ is the horn dominant region, and $200° < \phi < 310°$ is the combined horn–dipole region.

The horn dominant region ($30° < \phi < 200°$) in this plot shows the restriction of the measuring instrument whose scale is limited to ±180° for phase measurements; hence, the plot shows modulo 2π cuts of the total phase change of 3060°, which represents a frequency deviation about the carrier frequency of approximately 19 Hz (see Ref. 2).

Figure 12 is a comparison of the amplitude variation of the mathematical model versus the measurement data for one revolution of the spacecraft at the aspect angle of 45°. Figures 13, 14, and 15 are the comparisons of the same computer plot (at $\psi = 45°$) with measured data for $\psi = 44°$, 46°, 47°, respectively, using various values of E_H, E_D.

Using a scaled drawing of the spacecraft geometry for an aspect of $\psi = 50°$, the equation for β becomes

$$\beta_{50°} = [1820° (14.6 - 7.57 \cos\phi + \cos^2\phi)^{1/2}] + \phi - 4830° \quad (9)$$

Substitution of this value into Eq. (6) produces a computer plot as shown in Figs. 16, 17, and 18 comparing the measured plots for $\phi = 49°$, 50°, and 51°, respectively, again with various ratios of E_H/E_D.

In similar fashion Figs. 19, 20, and 21 are comparisons of the computer plot of the phase variation for $\psi = 45°$ against the measured data for $\psi = 44°$, 45°, and 46°. Figure 19 shows a frequency deviation region which is not covered by this model.

In Fig. 20, for the computer plot, the dipole antenna gain is constant ($E_D = 1$) and the horn antenna relative gain varied as a function of ϕ, i.e., $E_H = 1$ at $0° < \phi < 100°$, $E_H = 1.08$ at $100° < \phi < 190°$, $E_H = 0.7$ at $190° < \phi < 360°$ compared to the measured antenna plot. This illustrates the varying horn antenna gain versus the rotation angle ϕ (due to its offset symmetry axis) and clearly shows that the phase deviation has varying values for one spacecraft rotation. Notice the similarity to Fig. 11 for the amplitude case.

Figures 22, 23, and 24 compare the computer phase plot for $\psi = 50°$ against the measured data for $\psi = 49°$, 50°, and 51°, respectively, and, as seen in Figs. 8 and 9, the ratio of E_H/E_D is less than 1 and nearly constant.

VI. Evaluation of the Mathematical Model

If the good correlation of the mathematical model computer plots relative to the actual measurement plots is accepted as the validity of the model, to a first approximation, then an analysis of the model results should aid in the determination of the effects of the amplitude and spin modulation characteristics on the telecommunications link performance.

A study of Eq. (4) related to the carrier amplitude indicates that the coefficient to the circular function is compensating, i.e., when $E_H = E_D = 1$, the maximum peak-to-peak variation of the amplitude exists; when $E_D > E_H$, the peak variation decreases; and, similarly, when $E_H > E_D$, the peak variation also decreases. For example, Figs. 3 and 4 illustrate that the maximum peak variation exists at $E_H = E_D = 1$, and Figs. 4b and 4c show similar peak values when $E_D > E_H$ and $E_H > E_D$, respectively.

In the case of the phase function, however, the maximum phase deviation does not exist at $E_H/E_D = 1$ but does decrease at $E_H/E_D < 1$. For example, when $E_H/E_D = 0.7$, the peak-to-peak variation is ±46° as shown in Fig. 6. The sensitivity of the peak variation as E_H/E_D becomes greater than 1 is shown in Fig. 7, where the ratio $E_H/E_D = 1.08$ can be seen to nearly double the peak variation when $E_H/E_D = 1$. This indicates the domineering influence of the rotating horn antenna to phase variation.

For the combined horn–dipole region ($44 < \psi < 53°$), the phase variation upon the carrier was seen to be a mix of frequency deviation (which was tested in Ref. 1) and phase deviation. The phase deviation as shown in Fig. 20 can be assumed to be a sawtooth waveform with an

average periodic frequency of 25 Hz (since the spacecraft rotates at 1 cycle/s) with a phase deviation of ±150° maximum.

The Fourier series of a sawtooth waveform is expressed by

$$y = \frac{2}{\pi} E \left(\sin x - \frac{1}{2} \sin 2x + \frac{1}{3} \sin 3x + \cdots - \frac{1}{n} \sin nx \right) \tag{10}$$

where E is the peak-to-peak value of the waveform.

Thus, for the periodicity of 25 Hz average, the fundamental frequency component would produce a maximum phase deviation of $\pm 150° \times 0.636 = \pm 86°$ and a corresponding deviation of ±43° for the second harmonic component and ±28.6° for the third harmonic component. This results in sideband components spaced about the carrier frequency separated by integer values of 25 Hz with decreasing amplitude.

The question arises as to what effect these components have upon the RF phase-locked loop (PLL) whose threshold loop bandwidth values are 48 and 152 Hz (two-sided). This question will be discussed later.

In the dipole dominant region it was analyzed (Ref. 3) that phase deviation was largely due to the solar panels and dipole antenna misalignment. Thus, the total effect upon the carrier can be summarized as a mixture of frequency deviation and phase deviation as a function of the aspect angle ψ, as shown in Fig. 25.

Since the model was formulated from the physical dimensions and geometry of the spacecraft, the equations are easily adaptable to the uplink conditions and applicable because of reciprocity.

VII. System Test

A possible test of the Telemetry System performance, based on the results of the mathematical model, could be structured on the technique employed previously as in Ref. 1.

An addition to the previous test would be to evaluate separately the performance of the receiver phase-locked loop when subjected to the worst-case condition from the LGA interferometry. From the computer plots it was shown that the phase deviation, or phase modulation, upon the carrier was that of a sawtooth waveform occurring at a periodic rate of 25 Hz, producing a phase deviation of ±150° peak-to-peak. However, from the Fourier series, it was shown (Eq. 10) that the fundamental frequency results in an approximate ±86° phase deviation.

Since the resulting spectrum overlaps the effective receiver loop noise bandwidths ($2B_{L_0} = 48$ and 152 Hz), a good experimental test would be to see what this spectrum does to the degradation of PLL performance as a function of carrier signal-to-noise ratio (SNR).

Figure 26 is the block diagram of a possible arrangement to evaluate the receiver PLL. The function generator with a sawtooth pattern would phase modulate the exciter only at the periodic frequency of 25 Hz and level set to deviate the carrier ±150° peak-to-peak.

The input signal level to the receiver would then be adjusted to produce a decreasing SNR and then measure the number of cycles slipped by the PLL (for a given elapsed test run time). The procedure would be to initially obtain the cycle slippage characteristics without the perturbing interferometry signal followed by the phase modulation without amplitude modulation and then a repeat with the combined PM and AM applied.

Similar to previous tests, an actual telemetry signal would be applied and a value of the resultant symbol error rate (SER) versus input ST_{s_H}/N_0 determined.

VIII. Computer Program

The MBASIC conversational computer language was used to develop the mathematical model for the LGA. The program instruction was written in sentence form and then combined into a program module that was written like a paragraph.

Equation (6) for the signal amplitude, at $\psi = 45°$, was written as

$$E_S = E_D \left\{ 1 + \left(\frac{E_H}{E_D} \right)^2 + 2 \left(\frac{E_H}{E_D} \right) \cos \left[1660° \left(21.4 - 9.25 \cos \phi + \cos^2 \phi \right)^{1/2} + \phi - 5800° \right] \right\}^{1/2} \tag{6}$$

and the resultant plot of this program is shown in Fig. 27. A comparison of this plot against Fig. 3b (or measured data as in Fig. 15) indicated that there exists a phase reference error as seen by the envelope shape at $\theta = 180°$.

This discrepancy is probably due to the initial phase relation between the horn and dipole antenna signals assumed as shown in the vector summation diagram and projection diagram of Fig. 2. Since an unknown phase shift exists within the RF cables, power splitters, etc., the initial phase condition must be more closely approximated.

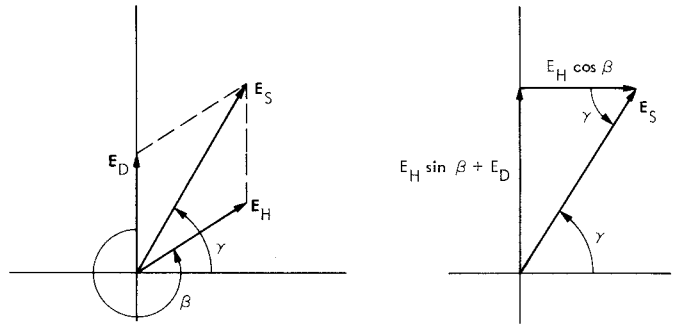

Assume then that at $\phi = 0°$ the horn phase is leading the dipole at a phase angle β greater than 270° as shown in the following diagrams:

---

then

$$\mathbf{E}_S = [(E_H \sin\beta + E_D)^2 + (E_H \cos\beta)^2]^{1/2} \tag{11}$$

and

$$E_S \angle \gamma = E_D \left[1 + \left(\frac{E_H}{E_D}\right)^2 + 2\left(\frac{E_H}{E_D}\right) \sin\beta \right]^{1/2} \angle \arctan\left(\frac{1 + \frac{E_H}{E_D} \sin\beta}{\frac{E_H}{E_D} \cos\beta} \right) \tag{12}$$

will be used as the general equation for the amplitude and phase relation of the summed signal.

Thus, the signal amplitude equation becomes

$$E_S = E_D \left\{ 1 + \left(\frac{E_H}{E_D}\right)^2 + 2\left(\frac{E_H}{E_D}\right) \sin\left[1660° \left(21.4 - 9.25\cos\phi + \cos^2\phi\right)^{1/2} + \phi - 5800°\right] \right\}^{1/2} \tag{13}$$

and for phase

$$\gamma = \arctan\left(\frac{1 + \frac{E_H}{E_D} \sin\left[1660° \left(21.4 - 9.25\cos\phi + \cos^2\phi\right)^{1/2} + \phi - 5800°\right]}{\frac{E_H}{E_D} \cos\left[1660° \left(21.4 - 9.25\cos\phi + \cos^2\phi\right)^{1/2} + \phi - 5800°\right]} \right) \tag{14}$$

for the aspect angle of 45°.

The final computer program for the amplitude is listed as follows:

```
55 INPUT USING 'A=#B=#C=#D=#':A,B,C,D&! ENTER COEFF FOR MODEL
60 FOR LOOP=1 UNTIL DONE WHERE DONE=0
65   INPUT USING 'MORE PLOT CASES (YES OR NO)?%':AN$
70   GO TO 170 IF DONE=1 WHERE DONE=(AN$='N')
90   INPUT USING 'ENTER VALUES FOR EH AND ED: # #':EH,ED
100  PRINT 'PLTL'
110  FOR PHI=0 TO 360 WHERE E=EH/ED
120    ES=ED*SQR(1+E**2+2*E*SIN(A*SQR(B-C*COS(PHI)+(COS(PHI))**2)-D+PHI))
130    PRINT USING '%%%% %%%%':9999*PHI/360,9999*((2+LOG10(ES))/2)*.48
```

```
140    NEXT PHI&
160    PRINT 'PLTT'
170    NEXT LOOP
```

In line 90, EH and ED are the magnitudes of the horn and dipole antenna gain respectively, with their gain ratio listed as E = EH/ED as in line 110.

The coefficients A, B, C, and D in line 120 are related to the geometrical dimensions obtained from Fig. 2b and the solution for L as explained by Eq. (2) for the case of $\psi = 45°$.

The resultant computer plots for the amplitudes are as shown in the previous figures.

The program for the resultant phase variation is listed below:

```
50  INPUT USING 'ENTER VALUES FOR EH1 AND ED1: # #':EH1,ED1
75  A1=1820,A2=14.6,A3=7.57,A4=4830
100 PRINT 'PLTL'     ! START OF PLOTTING
110 FOR PHI=0 TO 360 WHERE E=EH1/ED1
115   EN=E*COS(A1*SQR(A2-A3*COS(PHI)+COS(PHI)**2)+PHI-A4)
117   ED=1+E*SIN(A1*SQR(A2-A3*COS(PHI)+(COS(PHI))**2)+PHI-A4)
120   GAMMA=180+ATN(ED,EN) ! 180 IS ADDED FOR PLOTTING OF E>1 CASES
130   PRINT USING '%%%% %%%%':9999*PHI/360,9999*(GAMMA/180)*(2/4.25)
140   NEXT PHI
160 PRINT 'PLTT'     !TERMINATE PLOT
```

Again the gain values for the horn antenna, EH1, and dipole antenna, ED1, are entered (line 50). A1, A2, A3, A4 (line 75) are coefficients that are used in the solution for β (lines 115 and 117). These coefficients are the values obtained by scaling the diagram of Fig. 2b for $\psi = 50°$.

EN (line 115) and ED (line 117) are the numerator and denominator expressions of Eq. (14).

The general equation GAMMA = ATN (ED, EN) served when $E_H < E_D$, since by Eq. (8), the resultant angle, γ, never exceeded 90°; however, when $E_H > E_D$, gamma is greater than 90° and the program included a modifier for this condition by the prefix addition 180 as stated in line 120.

References

1. Ham, N. C., "Amplitude and Frequency Modulation Effects to Telemetry Link Reception," in *The Deep Space Network Progress Report*, Technical Report 32-1526, Vol. XIV, pp. 149–160, Jet Propulsion Laboratory, Pasadena, Calif., Apr. 15, 1973.
2. Ham, N. C., *Helios LGA Pattern Measurements*, IOM 335A-73-113, Mar. 21, 1973 (JPL internal document).
3. Zerwes, G., *Radiation Characteristics of Helios Low Gain Antenna*, Technical Memorandum RB1-6764/73 C-264, Messerschmitt-Bokow-Blohm, Ottobrunn, W. Germany, Mar. 26, 1973.

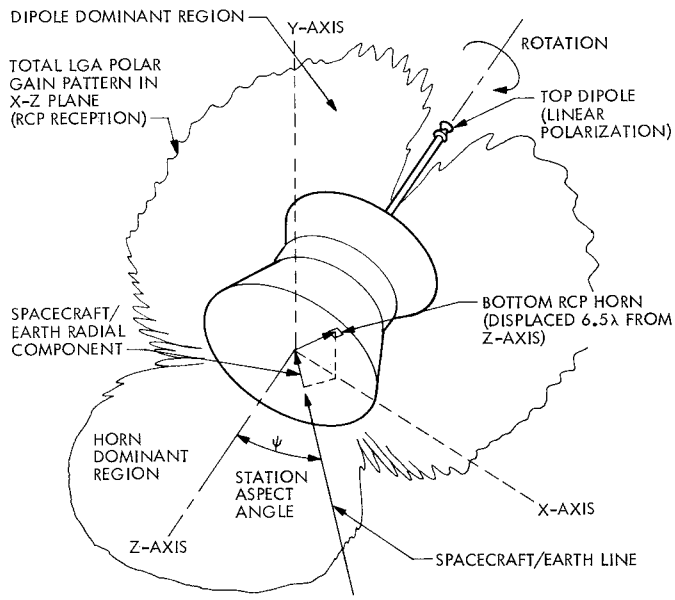

Fig. 1. Spacecraft coordinate configuration

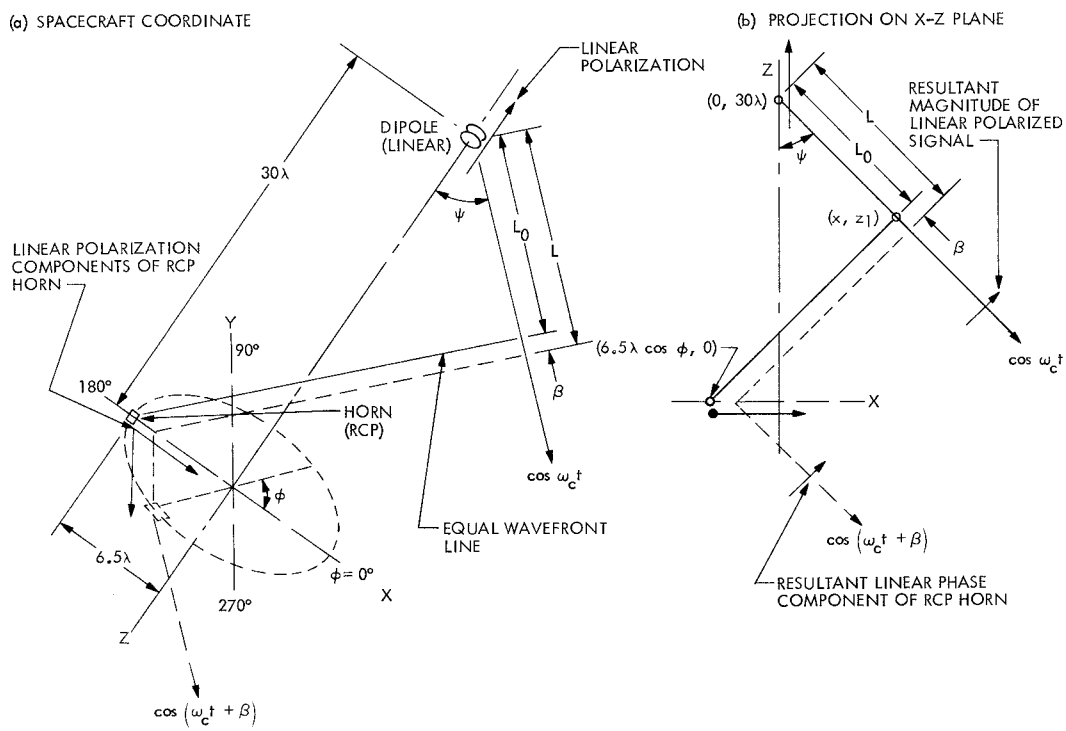

Fig. 2. Spacecraft LGA interferometry

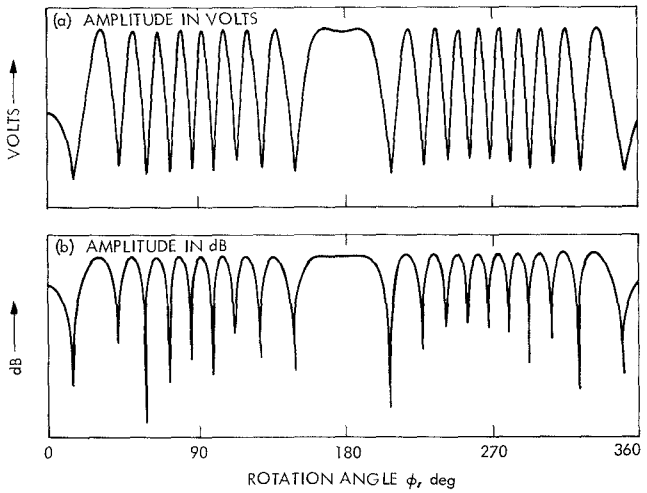

Fig. 3. Computer plots of carrier amplitude, $\psi = 45°$, $E_H = 1$, $E_D = 1$

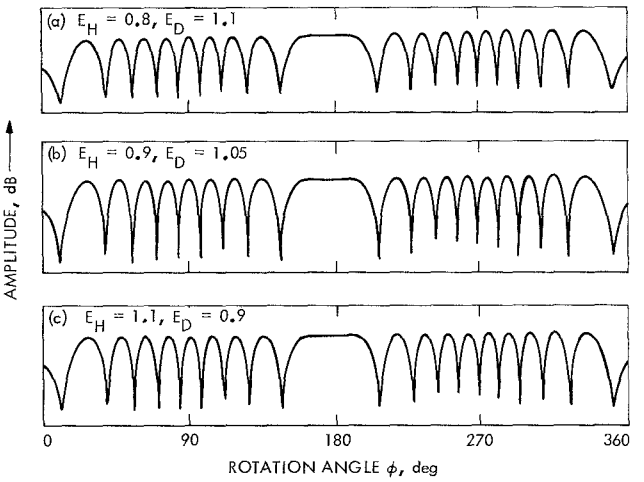

Fig. 4. Computer plots of carrier amplitude, $\psi = 45°$

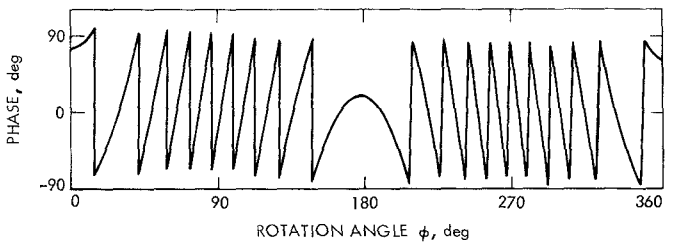

Fig. 5. Computer plot of carrier phase, $\psi = 45°$, $E_H = 1$, $E_D = 1$

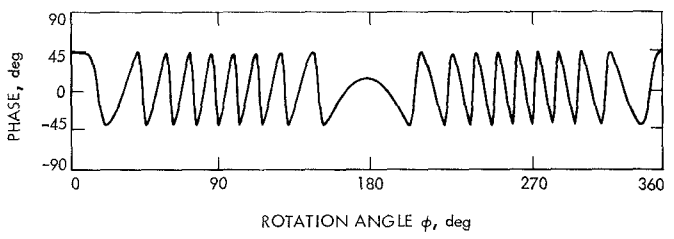

Fig. 6. Computer plot of carrier phase, $\psi = 45°$, $E_H = 0.7$, $E_D = 1$

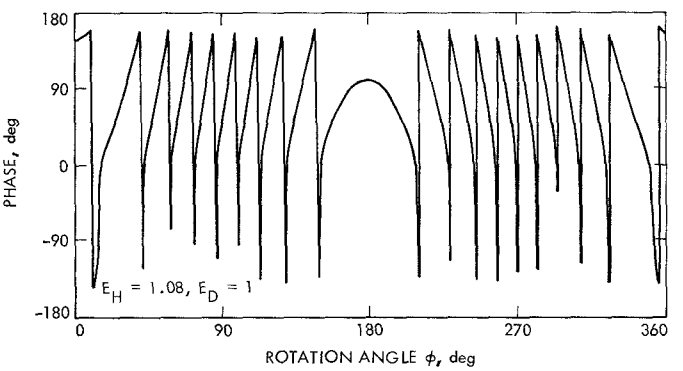

Fig. 7. Computer plot of carrier phase, $\psi = 45°$

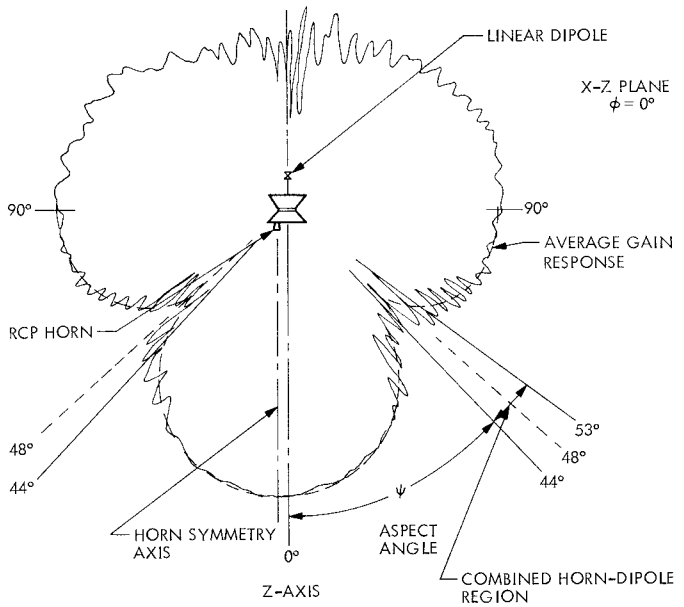

Fig. 8. Polar plot of LGA for RCP reception (downlink frequency)

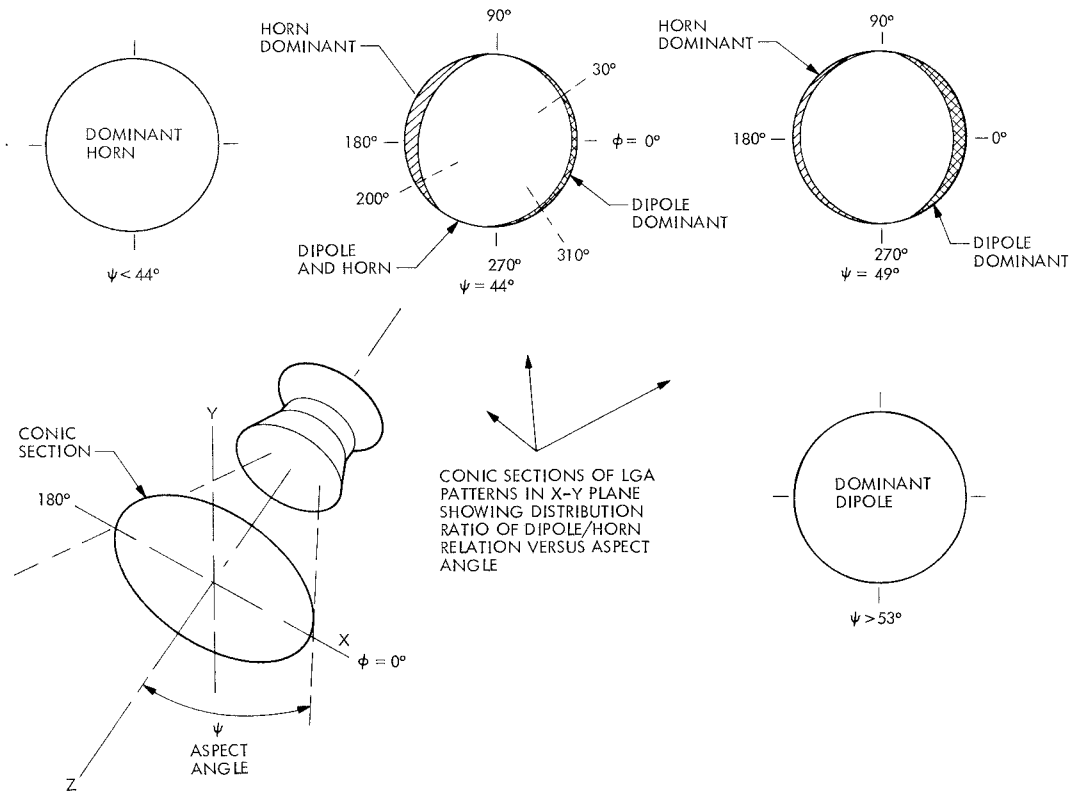

Fig. 9. LGA conic section pattern versus aspect angle

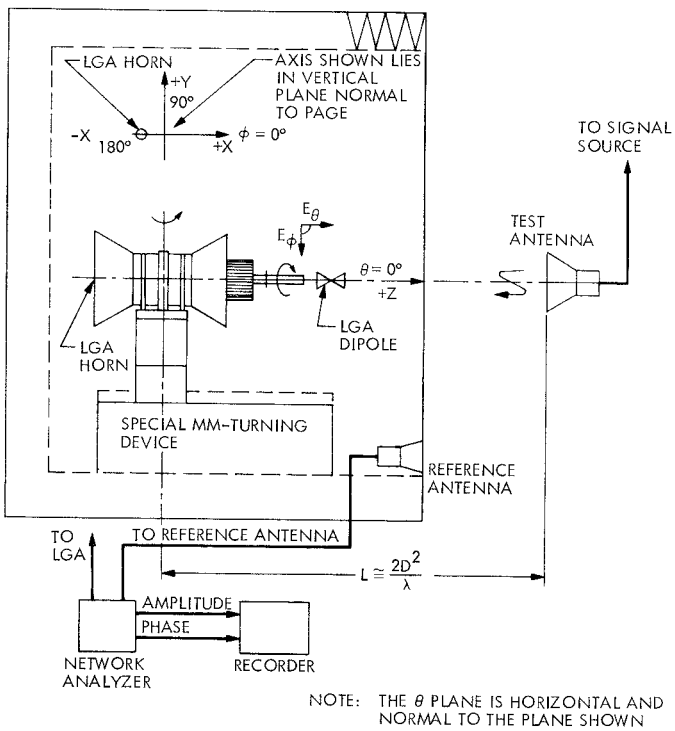

Fig. 10. Radiation pattern test setup

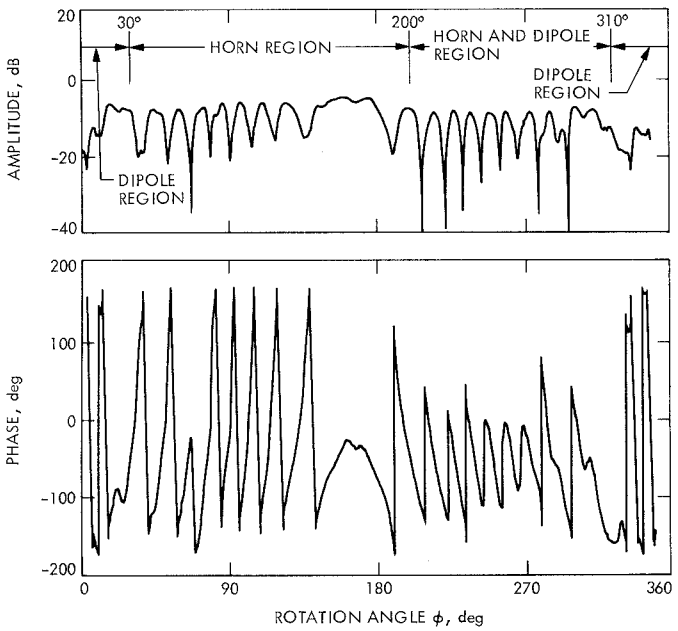

Fig. 11. Helios LGA measured data, $\psi = 44°$

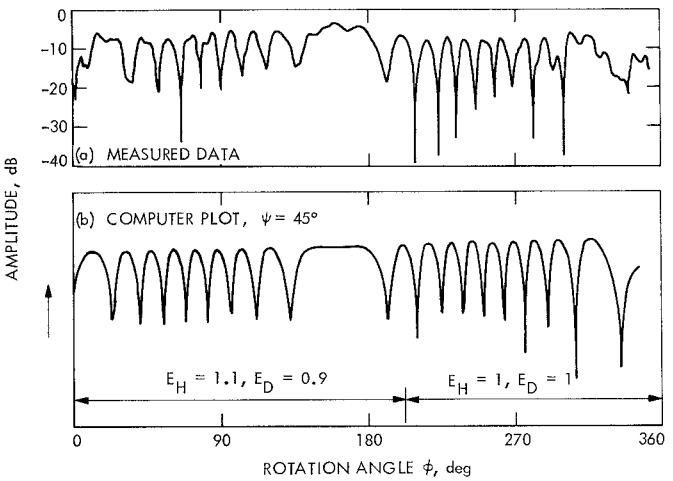

Fig. 13. Computer plot versus measured data, $\psi = 44°$

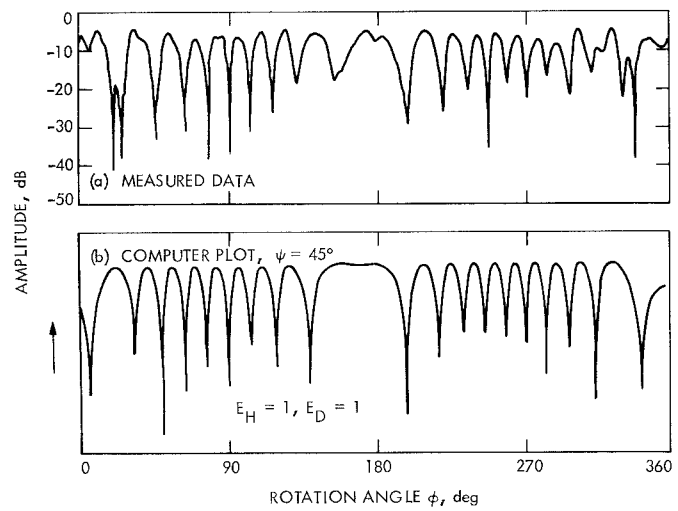

Fig. 12. Computer plot versus measured data, $\psi = 45°$

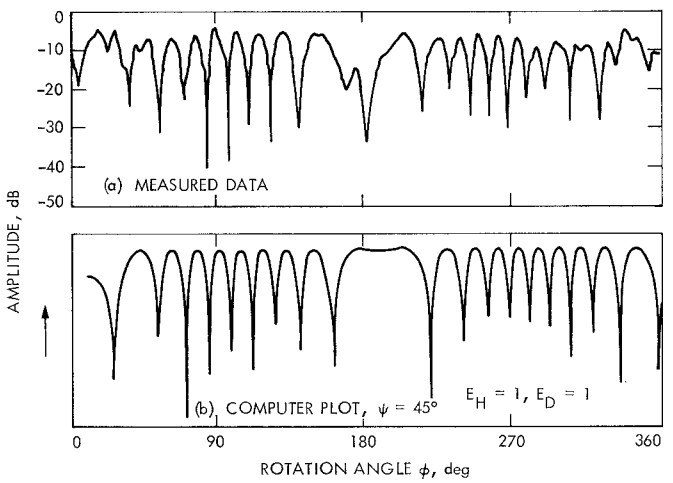

Fig. 14. Computer plot versus measured data, $\psi = 46°$

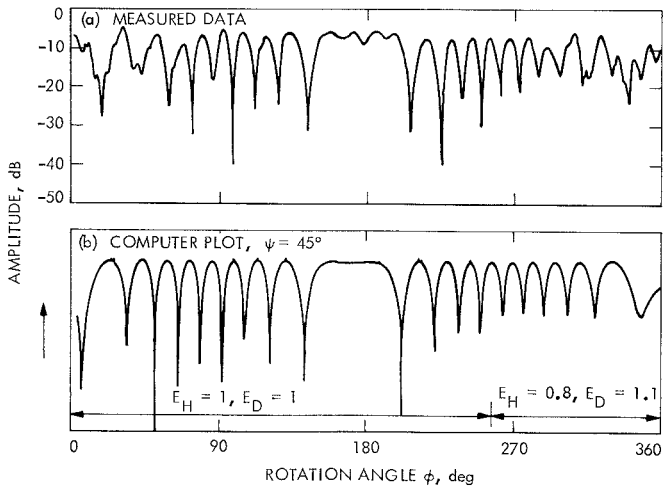

Fig. 15. Computer plot versus measured data, $\psi = 47°$

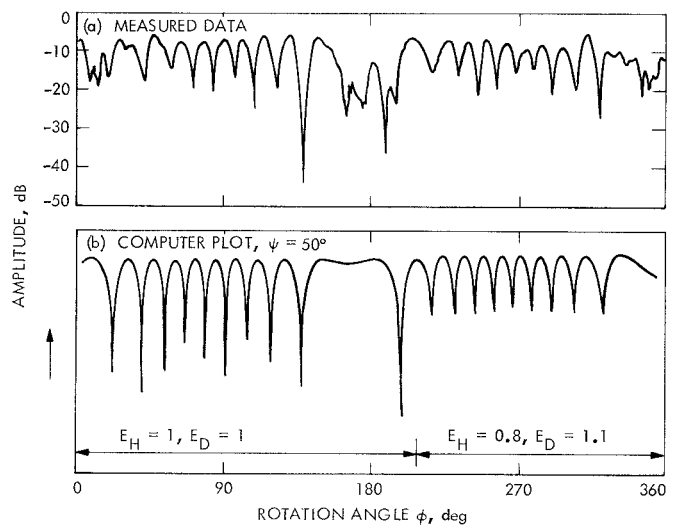

Fig. 16. Computer plot versus measured data, $\psi = 49°$

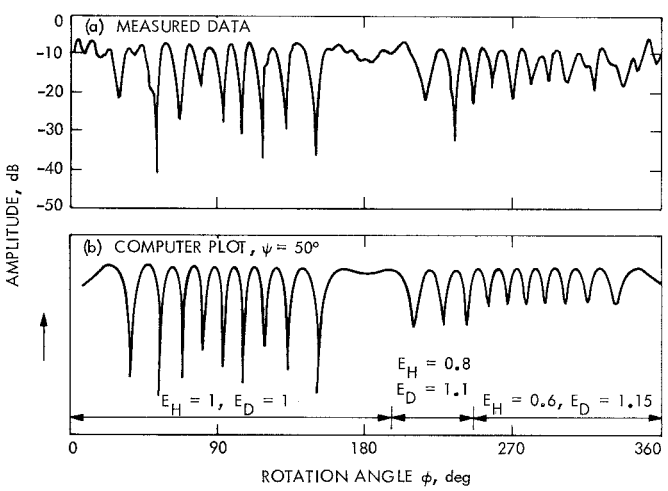

Fig. 17. Computer plot versus measured data, $\psi = 50°$

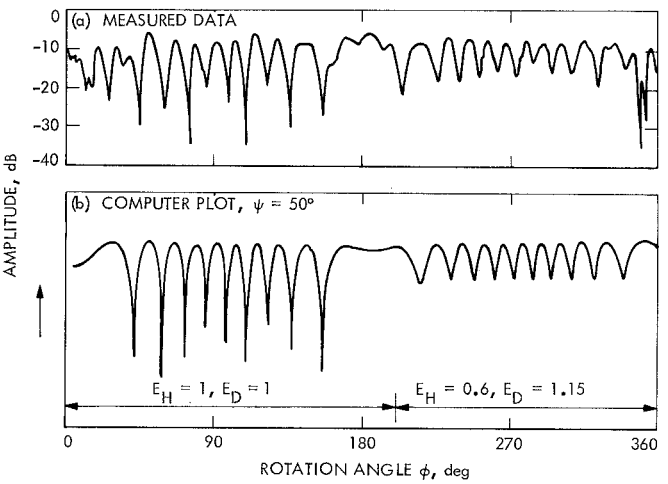

Fig. 18. Computer plot versus measured data, $\psi = 51°$

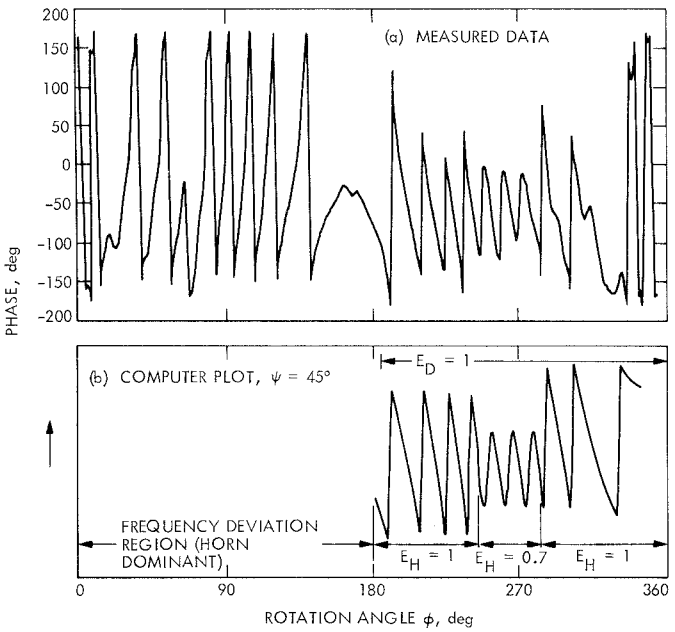

Fig. 19. Computer plot versus measured phase data, $\psi = 44°$

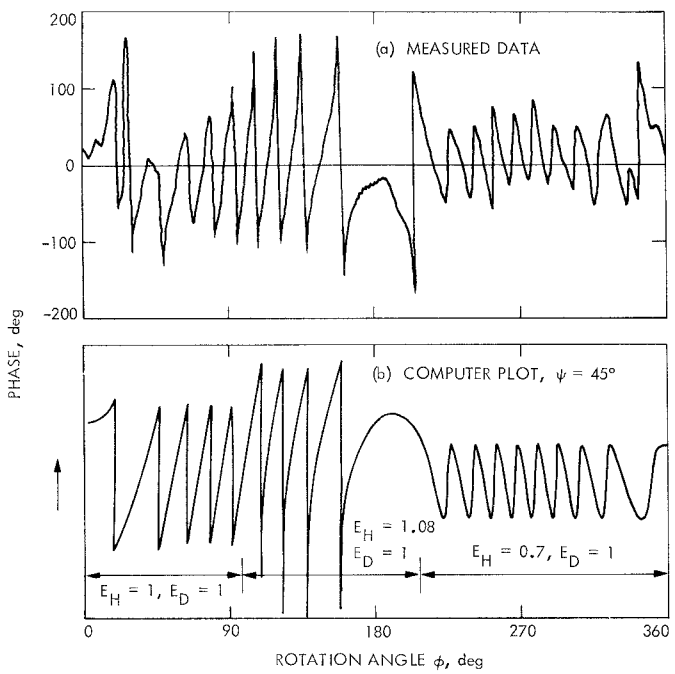

Fig. 20. Computer plot versus measured phase data, $\psi = 45°$

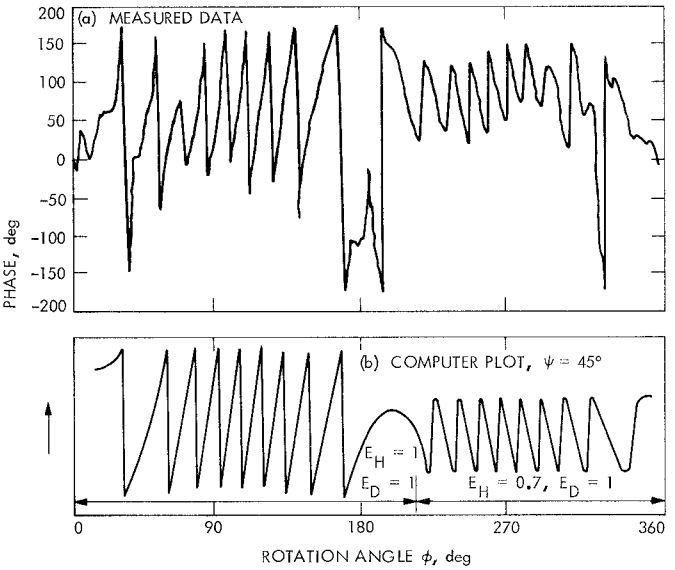

Fig. 21. Computer plot versus measured phase data, $\psi = 46°$

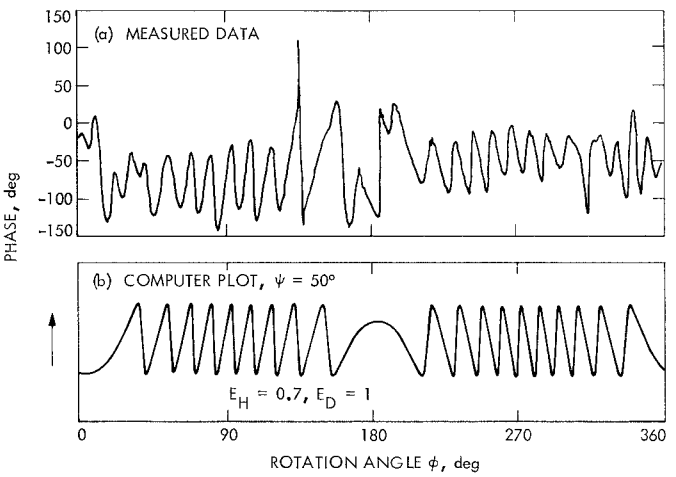

Fig. 22. Computer plot versus measured phase data, $\psi = 49°$

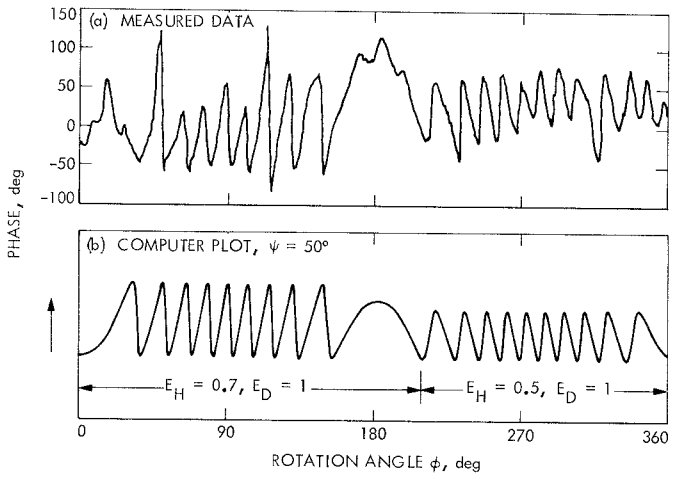

Fig. 23. Computer plot versus measured phase data, $\psi = 50°$

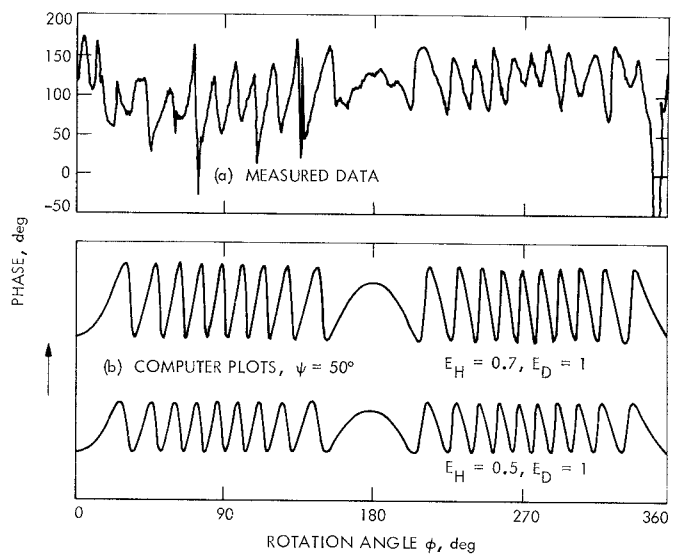

Fig. 24. Computer plots versus measured phase data, $\psi = 51°$

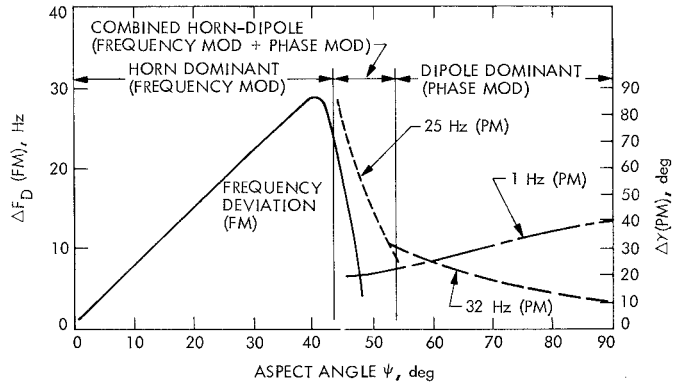

Fig. 25. Frequency deviation and PM versus aspect angle for RCP reception

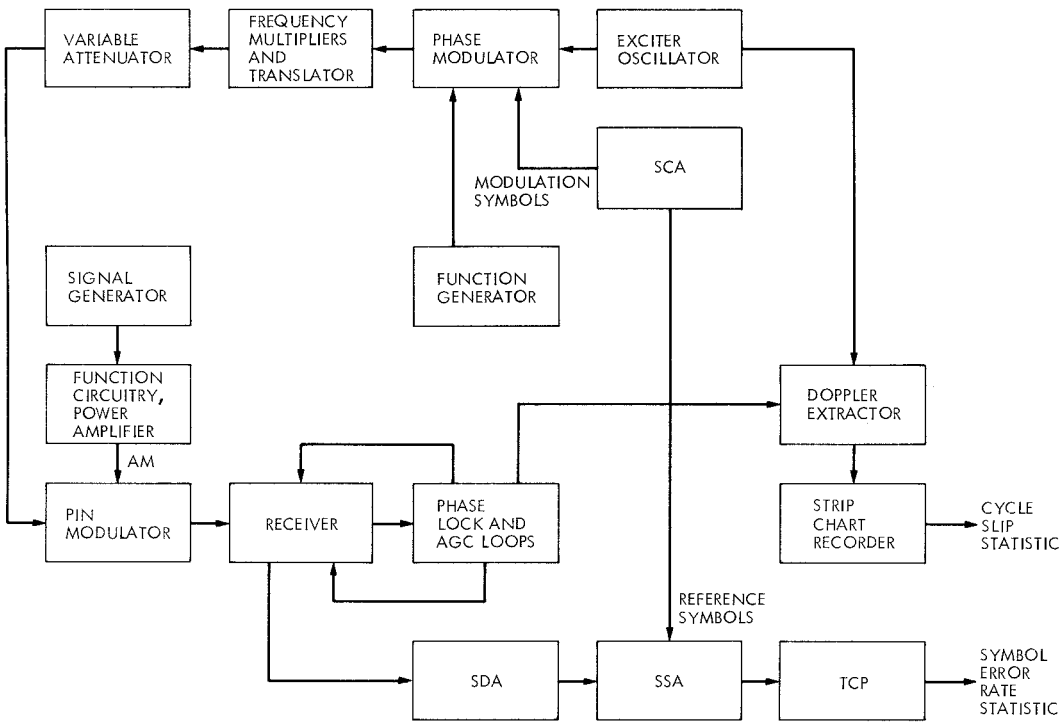

Fig. 26. Block diagram of system test configuration

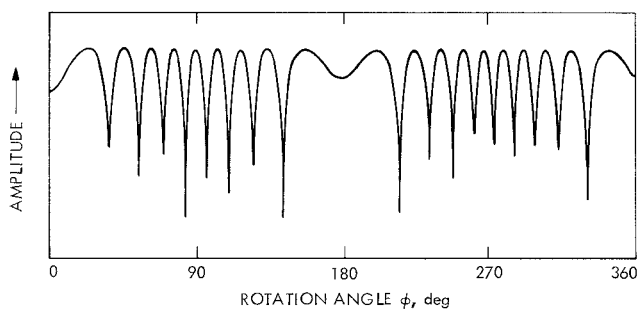

Fig. 27. Computer plot of amplitude, $\psi = 45°$